Optimal Foot Location for Placing Wearable IMU Sensors and Automatic Feature Extraction for Gait Analysis

Arif Reza Anwary, Hongnian Yu, *Senior Member, IEEE*, and Michael Vassallo

***Abstract*— Our aim is to maximize the interpretable information for gait analysis. To achieve this, it is important to find the optimal sensor placement and the parameters that influence the extraction of automatic gait features. We investigated the effect of different anatomical foot locations on inertial measurement unit (IMU) sensor output. We designed and developed an android app to collect real-time synchronous sensor output. We selected a set of five anatomical foot locations covering most of the foot regions to place wearable IMU sensors for data collection. Each participant performed a trial in a straight corridor comprising 25 strides of normal walking, a turn-around, and another 25 strides. We proposed an automatic gait features extraction method to analyze the data for stride number, distance, speed, length and period of stride, stance, and swing phases during walking. The highest accuracy for detecting stride number was in location 1 (first cuneiform) followed by location 5 (Achilles Tendon) and 4 (Talus). Location 1 was the closest to correlate estimate to the measured distance travelled. The accuracy of detecting number of strides on average is 95.47% from accelerometer data and 93.60% from gyroscope data and closest to the 60:40% split for average stance and swing for 15 subjects. To validate our results, we conducted trials using the Qualisys motion capture instrument and from our sensors concurrently. The average accuracy of the result is 97.77% with 95% confidence interval 0.767 for estimated and 99.01% with 95% confidence interval 0.266 for period.**

***Index Terms*— Inertial measurement unit (IMU), accelerometer, gyroscope, sensor placement, optimal location, feature extraction, wearable sensors, gait analysis.**

I. Introduction

GAIT analysis provides information about human locomotion including step length, stride length, stance and swing length, speed, step angle, hip angle and other information [1]. It is employed in different domains such as sports, rehabilitation, and health diagnostics. It has different sports applications to improve athlete's performance, sports training [2] and to prevent injury. It is also used to monitor patient progress in orthopaedics and rehabilitation [3]. In biometrics and biomedical engineering areas, gait analysis is used as a fundamental method and assistive tool to characterize human locomotion and has many applications [4]. Gait analysis is also important for fall risk assessment of elderly patients [5] as well as the prediction [6], detection [7] and prevention of falls [8]. It is also a predictor of functional and cognitive decline [9], [10]. Gait disorders are common in older people due to physiological age related changes in the musculoskeletal system as well as increased prevalence of several diseases promoting postural instability [11]. Importantly, gait disturbances may also be a marker of the development of Parkinson's disease [12], cardiovascular disease [13], diabetic neuropathy [14] and dementia [9], [15].

To perform gait analysis, the collection of gait parameters is crucial. The conventional scales used to analyze gait parameters in clinical assessment are mainly subjective or semi-subjective. Different assessment tools such as the Gait Abnormality Rating Scale [16], Figure of 8 Walk Test [17], Four Square Step Test [18], The Functional Gait Assessment (FGA) [19], Groningen Meander Walking Test [20] and Berg Balance Scale [21] are used to observe the quality of a patient's gait and balance. However, these methods are subjective measurements with a high chance of intra and inter observer variation and human error. This may affect the accuracy of diagnosis, follow-up and treatment of the pathologies concerned [1].

A more objective way of assessing gait is required. There are a variety of wearable sensors including an accelerometer, gyroscope, magnetometer, foot pressure sensor, inclinometer, and goniometer [22] that are generally used to measure various characteristics of human gait. IMU sensors have been used in different gait analysis techniques such as monitoring of post-operative gait abnormalities [23], detection of falls [24], fall-related gait characteristics measured on a treadmill and in daily life [25], nature of Parkinsonian gait [26], auto-detection of daily living activities of older adults [27] and human waking foot trajectory [28]. These sensors are worn or attached directly or indirectly to different body locations such as foot, wrist, chest and head, and are attached using belts, clips or other accessories [29].

Various factors can affect the signal input and output. For example, during locomotion, movement of clothes can cause interference with accelerometer output [30]. There can be vibration or momentum noise if the sensor is not

Manuscript received November 13, 2017; accepted December 6, 2017. Date of publication January 4, 2018; date of current version February 21, 2018. This work was supported by European Commission funding ERASMUS MUNDUS FUSION (545831-EM-1-2013-1-IT-ERAMUNDUSEMA21) and Marie Skłodowska-Curie SMOOTH (H2020-MSCA-RISE-2016-734875) projects. The associate editor coordinating the review of this paper and approving it for publication was Dr. Edward Sazonov. *(Corresponding author: Hongnian Yu.)*

A. R. Anwary and H. Yu are with the Faculty of Science and Technology, Bournemouth University, Poole BH12 5BB, U.K. (e-mail: manwary@bournemouth.ac.uk; yuh@bournemouth.ac.uk).

M. Vassallo is with Royal Bournemouth Hospital, Bournemouth BH7 7DW, U.K., and also with the Centre of Postgraduate Medical Research and Education, Bournemouth University, Poole BH12 5BB, U.K. (e-mail: michael.vassallo@rbch.nhs.uk).

This paper has supplementary downloadable multimedia material available at http://ieeexplore.ieee.org provided by the authors. The Supplementary Material contains material that is not included within the paper itself. This material is 16MB in size.

Digital Object Identifier 10.1109/JSEN.2017.2786587

attached properly. Attaching the sensor with a belt or keeping in a pocket can also induce relative motion interference [31]. To increase the reliability and validity of automatic feature extraction from gait parameters for gait analysis, the influence of sensor location and attachment has to be determined. Further study on the best location for sensor placement is therefore required [32].

In this paper, we investigated the optimal location and orientation of placing an IMU sensor on the barefoot and the parameters that influence the automatic extraction of gait features. Research into accelerometer based gait parameters such as times of stance, swing, single and double support [33]; stride length and stance phase [34]; gait velocity, stride duration, cadence and step length [35]; step number, moving distances, instant step speed and average speed [36]; step counting [37]–[39]; times of heel strike, toe strike, heel-off, and toe-off [40]; stride length and duration [41]; walking distance, time and speed [42] were investigated. However, a low cost multi-sensor based synchronous data collection system for a comprehensive physical gait analysis totaling ten parameters has to our knowledge not been reported so far. We developed an android app for collecting synchronous information and an automatic gait features extraction method to extract features on stride number, total distance, total speed, stride length, stride period, stance length, stance period, swing length, swing period and ratio of stance and swing events, using low cost wearable IMU sensors.

The paper is organized in the following sections. Section II presents our design and the architecture of the proposed system. This includes the sensor placing location, sensor selection, android app design and development, and data collection. Section III gives the proposed method, which includes raw data processing, velocity and distance calculation, stride event detection, stance and swing events detection and gait features extractions. Section IV delivers the experimental results for 15 participants to demonstrate the proposed architecture and method, and the discussions. The conclusion is given in section V.

II. Design and Architecture

Figure 1 illustrates the architecture of the study identifying the various stages and processes involved.

A. Sensor Placing Location

The output of an accelerometer depends on the position at which it is placed, its orientation, posture, and activity being performed [43]. The signal also varies depending on the position on the foot [44]. We found that placing a sensor in different foot locations gave different signal patterns and affected sensor output.

In order to increase the sensor output accuracy and reliability, and reduce the variability, all sensors are fitted tightly to the barefoot. The sensors do not need to be worn in a perfectly upright position as this is not user-friendly and very hard to achieve. Any discrepancy between the sensor, foot and earth frame, is compensated using transformation of the sensor frame to earth frame assuming that the relative movement between the sensor frame and foot frame is negligible.

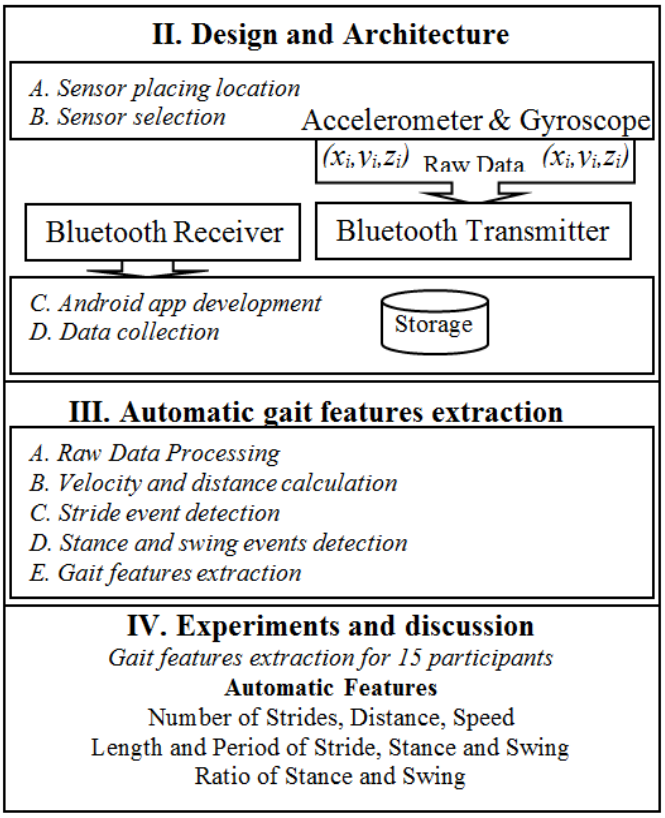

Fig. 1. Architecture of the proposed system.

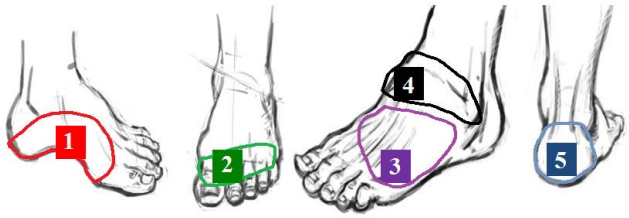

Fig. 2. Proposed IMU sensor placement of participants to five barefoot locations 1) metatarsal, 2) proximal phalange, 3) side metatarsal, 4) talus and 5) Achilles tendon.

We chose the barefoot rather than sensors attached to a shoe because wear and tear in the shoe can affect the position of the sensor and accuracy of the data output.

Accelerometer and gyroscope data were collected by placing the sensors in five selected foot locations that covered all of the regions of the barefoot (Fig. 2): the positions were chosen to include the medial, lateral, anterior dorsal, posterior dorsal and posterior of the foot. The plantar aspect is not covered as this is the part of the foot in contact with the floor and is not practical for the subject to walk on the sensor.

Location 1 - Medial aspect of foot over the bony prominence of the first cuneiform: This location is chosen to provide stability to the sensor and minimize its movement during motion of the foot.

Location 2 – Anterior dorsal aspect of foot over the second Metatarso pharyngeal joint: It is a flexible part of the foot during motion.

Location 3 - lateral aspect of foot over the base of the 5th metatarsal: The location is a flexible part of the foot during motion.

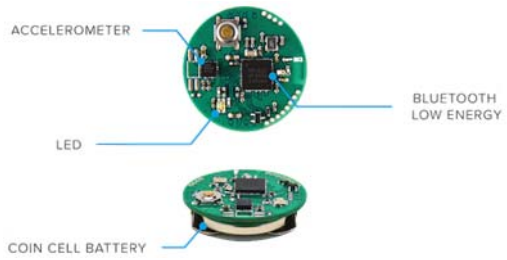

Fig. 3. IMU sensor MetaWear CPro [34].

Location 4 – Posterior dorsal over the Talar dome anterior to the ankle joint: It is a mobile part of the foot.

Location 5 - Achilles tendon: over the insertion of the Achilles tendon into the calcaneum, evaluates sensor data from the posterior aspect of the foot. As the sensor is placed over the calcaneum it is considered a relatively stable part of the foot during motion.

B. Sensor Selection

Selecting a sensor should have generic considerations such as protection from pressure, water and temperature, and the battery life.

There are wearable wireless IMU sensors commercially used for health rehabilitation, activity monitoring [45], [46], sports tracking or research. A list of available commercial IMU sensors are available from [47]. A wireless wearable Bluetooth, long autonomy, minimum consumption, multiple synchronized data transmission supported IMU sensor of low cost was important for our investigation. With all these considerations the recently introduced, Bluetooth Low Energy (BLE) based IMU sensor MetaWear CPro [63] was chosen. The power consumption of our sensor was low during sleep mode and high during operation mode. The sensor was in an active state when connected by Bluetooth to our android device and only went to sleep mode once it was disconnected.

This sensor, introduced by MbientLab, Portola, San Francisco, CA, 94134 USA, was used to collect synchronous accelerometer and gyroscope data. It is sensitive to acceleration and rotatory movements that occur during normal human locomotion (Fig. 3). It has a 32-bit ARM Cortex-M0 SOC - nRF51822 CPU, Embedded 2.4GHz BLE transceiver, radio-peak currents below 10 mA 3V, and powered by a coin-cell battery. It has internal 256K FLASH /16K RAM, BOSCH BMI160 accelerometer + gyroscope, BOSCH BMP280 barometer + temperature, Lite-On LTR329 light sensor, BOSCH BMM150 magnetometer, temperature sensor, indicator LEDs, and GPIOs / I2C. The board is 24mm diameter × 7.0mm height. Sensor data can stream at up to 100Hz using the Bluetooth Low Energy link and log up to 10K entries of sensor data at 800Hz in the MetaWear memory. The price was $30.00.

The sensor has a high accurate BOSCH BMI160 component which is a 6-axis IMU comprised of a 16-bit accelerometer and an ultra-low power gyroscope with an amplitude up to ±16g (S_{8g} sensitivity 4096 LSB/g) and a range of 2000 degrees/sec (R_{FS500} sensitivity 65.6 LSB/deg/sec) with a frequency up to 1600Hz (Fig. 3). It can achieve 99% accuracy. Investigation showed that IMU based sensors are sampled at a frequency range of 20Hz to 200Hz [48]. In practice, a low sampling rate for the accelerometer possibly produces excellent recognition and accuracy in posture and activity classification [49], [50]. In [50] acceleration data were sampled at 25Hz, in [51] data were sampled at 32Hz and in [52] at 50Hz. For this study, the accelerometer range was set to ±8 m/s^2 and gyroscope range was set to ±500 degs/s. The sampling rate of data collection was set to 50Hz. A casing for the MetaWear sensor was designed using SolidWorks [53] and printed using a 3D printer. A Velcro elastic belt and buckles were used to adjust and attach the sensor (Fig. 4).

Fig. 4. Proposed MetaWear casing, Velcro elastic belt, buckles and sensor placement on foot.

C. Android App Development

The MetaWear CPro sensor provides an Android API library for interacting with the MetaWear board on an Android mobile phone. A minimum of Android 4.3 (SDK 18) is required to use this library, however some features will not function properly due to the underlying Bluetooth LE (BLE) implementation. To get the best results, it was recommended to use an Android 4.4 (SDK 19) or higher. MetaWear CPro uses BLE 4.0. Based on these criteria, we designed and developed an Android app using Android Studio 2.2 to collect real time data from the MetaWear sensor. The HTC M9 mobile phone which has BLE 4.1 was used to connect to multiple MetaWear Cpro sensors. This mobile phone supported up to 7 MetaWear Cpro devices and it was able to collect synchronous data. The app collected accelerometer and gyroscope data, and stored data on an external SD card as a csv file. The data storing format in the csv file is date (*dd/mm/yyyy*), time (*HH:MM:SS.ss*), system clock (Millisecond), accelerometer (*X, Y, Z*) and gyroscope (*X, Y, Z*). The screenshot of the android app is shown in Fig. 5.

Initially the SCAN button on the app was pressed to find all the MetaWear CPro devices available for data collection. The order of data collection was selected by the Slot number. Each sensor then automatically connected with the corresponding mac address by showing "CONNECTED". Once the DATA RECORDING switch was pressed, a dialog box appeared prompting for a file name. Data collection started when the "OK" button was pressed. When the "STOP" button was pressed, the collected data was stored as a CSV file.

D. Data Collection

In natural walking the head, torso and hips are synchronized in a smooth bouncing vertical motion with each step. This vertical motion is in the same direction as the earth's gravitational force. Legs do most of the work during walking as

Fig. 5. Proposed android app to collect data from MetaWear CPro.

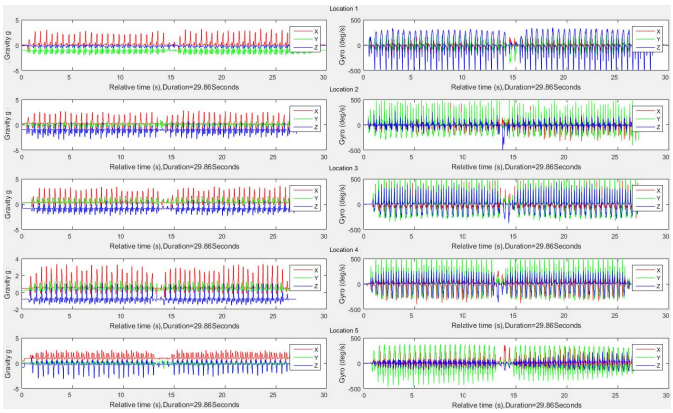

Fig. 6. Raw accelerometer and gyroscope data from test subject 1 for five locations.

the joints produce greater ranges of motion to move the body forward in the horizontal direction. This repetitive movement involves steps and strides known as the gait cycle. A stride is a whole gait cycle with stance and swing events [54]. This horizontal movement produces high acceleration and this is the movement investigated in this study. An accelerometer and a gyroscope are used to collect this horizontal movement information and then data are analyzed using our proposed method to find strides, stance and swing event information. The raw data from the accelerometer and gyroscope for location 1 to location 5 is presented in Fig. 6 and will be analyzed in Section III.

III. Automatic Gait Features Extraction

A. Raw Data Processing

To provide a robust absolute orientation vector in the form of Quaternion or Euler angles, the MetaWear CPro sensor combines the measurements from the 3-axis accelerometer and 3-axis gyroscope sensor. The algorithm from MbientLab [55] fuses the sensor raw data in an intelligent way to improve each output. This includes offset calibration of each sensor,

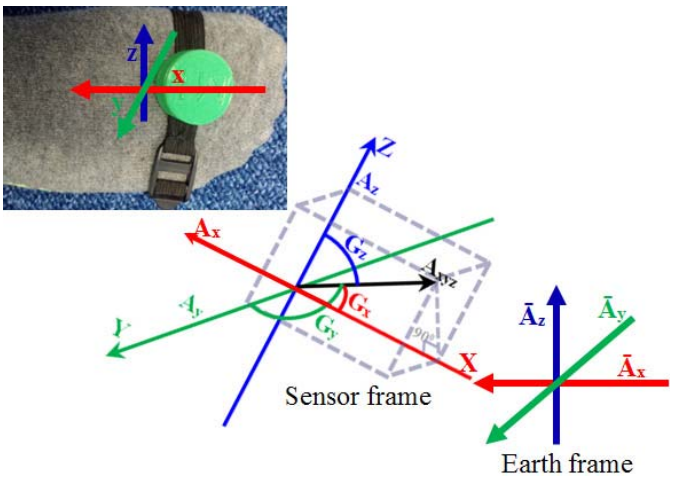

Fig. 7. Three dimensional IMU axes (*XYZ* is the foot coordinate; $\bar{A}_x\bar{A}_y\bar{A}_z$ is the earth coordinate).

monitoring of the calibration status and Kalman filter fusion to provide distortion-free and refined orientation vectors [55]. The IMU sensor gives three dimensional accelerometer data A=[a_x, a_y, a_z] and gyroscope data G=[g_x, g_y, g_z] with respect to time t. As the accelerometer is sensitive to linear acceleration due to movement and the local gravitational force, the input data consists of user acceleration and gravitational acceleration. The user movement will result in positive data towards the a_x, a_y, and a_z axis of the sensor and, by convention, these are defined so that a linear acceleration aligned in the direction of these axes will give a positive acceleration output. Again a gravitational force component aligned along the same axes directions will, however, result in a negative reading on the accelerometer.

In this study, there are three coordinate systems: the foot frame, the sensor frame and the earth frame. Since the sensor is attached to the foot tightly, the sensor does not slip or move during walking time. The relative movement between the sensor frame and foot frame is assumed to be negligible; hence the foot frame and sensor frame are treated as a same frame. The sensor frame and the earth frame are the two coordinates and the sensor frame should be transferred to the earth frame and remove gravitational component. The A_x axis is aligned along the foot axis of the IMU sensor, the A_z axis points downwards so that it is aligned with gravity and the A_y axis is aligned at right angles to both A_x and A_z axes so that the three axes from a right handed coordinate system are shown in Fig. 7.

There are many conventional methods to split the gravitational component from accelerometer data and three of them [56]–[58] were investigated. Madgwick [56] used a frequency of 256 Hz with a gain factor of 0.1. For our data the sampling frequency was 50 Hz. The convergence was fast but angles were more susceptible to linear accelerations and the output drifted. A similar error of linear accelerations was found using the Mahony method [57]. The method developed by Mizell [58] was then used to estimate the vertical component and the magnitude of the horizontal component of the user's motion. The average initial gravity component on each axis

was estimated at standing position before starting to walk. Thus the initial gravity acceleration vector $[\bar{a}_x, \bar{a}_y, \bar{a}_z]$ consisted of the average magnitude of n samples of accelerometer data and was estimated using equation (1),

$$\bar{A} = \left[\bar{a}_x, \bar{a}_y, \bar{a}_z\right] = \frac{1}{n}\sum_{i=1}^{n}\left[a_{x_i}, a_{y_i}, a_{z_i}\right] \tag{1}$$

where $i = 1, 2, 3, \ldots, n$ and $n = 10$. It was noted that initially the earth frame and the foot frame were the same. Here $\bar{A}$ was used as the acceleration under the earth frame. The dynamic component of the acceleration estimated using equation (2) was due to user motion rather than gravitational force.

$$A_d = [d_x, d_y, d_z] = [a_x - \bar{a}_x, a_y - \bar{a}_y, a_z - \bar{a}_z] \tag{2}$$

where A_d was the acceleration under the foot frame. The projection A_p of A_d on the axis $\bar{A}$ using equation (3) [58]

$$A_P = \left(\frac{A_d \bullet \bar{A}}{\bar{A} \bullet \bar{A}}\right)\bar{A} \tag{3}$$

In equation (3), A_p was the projection component of the dynamic acceleration vector A_d on $\bar{A}$. As a three-dimensional vector consisted of its vertical and horizontal components, the horizontal component A_h of the dynamic acceleration was computed using equation (4)

$$A_h = A_d - A_p \tag{4}$$

The conversion of the accelerometer from gravitational force g to user acceleration of movement (AM) m/s^2 was $AM_{xyz} = A_h * 9.81$ where AM_{xyz}=$[am_x, am_y, am_z]$. The three axis data were transformed due to the fact that mapping at specific axes was sensitive to the sensor orientation [59]. If the data were mapped on each axis individually, small changes in orientation or attached location may erroneously be flagged as a change in movement. The sensor orientation and attachment were maintained using a small casing and Velcro elastic buckles, every time the sensor was attached. We aimed to put in the same orientation even though a different orientation would have given similar results. The acceleration of total A_{xyz} and gyroscope G_{xyz} towards three axes *x, y* and *z* directions were estimated by using equations (5) and (6).

$$\left|A_{xyz_i}\right| = \sqrt{am_{x_i}^2 + am_{y_i}^2 + am_{z_i}^2} \tag{5}$$

$$\left|G_{xyz_i}\right| = \sqrt{g_{x_i}^2 + g_{y_i}^2 + g_{z_i}^2} \tag{6}$$

The preliminary experimental data were collected in this section from one male subject age 35 years old, height 1.72m and weight 73kg to develop and demonstrate our method. At this stage of the experiment the aim was to prove the concept and that data can be collected and analyzed. It was not intended to generate conclusions about the optimal location for placing sensors. The total walking distance was measured offline and then compared with the calculated distance. The wearable MetaWear CPro sensors were placed in five different locations on the right foot. The subject performed a trail in a straight corridor walking on a hard floor. The trail comprised of 25 strides of normal walking, a turn-around and another 25 strides. The distance was measured by a tape and the

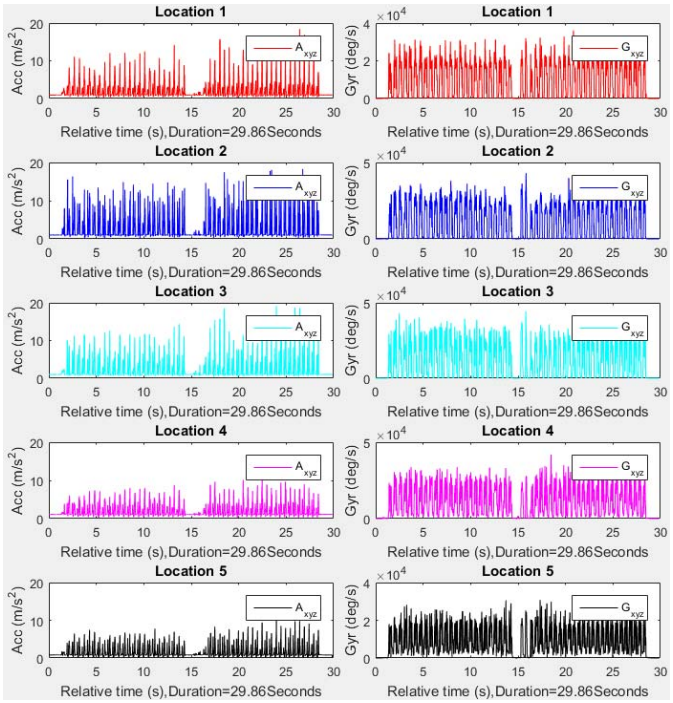

Fig. 8. Total acceleration A_{xyz} and gyroscope G_{xyz} towards three axes *x, y* and *z* directions from Location 1 to 5.

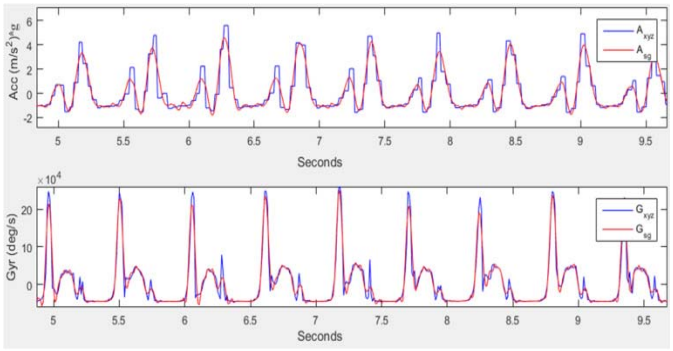

Fig. 9. Original (A_{xyz} and G_{xyz}) and filtered (A_{sg} and G_{sg}) acceleration and gyroscope data using Savitzky-Golay.

Android app was used to record the time. For example, for the data from this subject, total acceleration $\left|A_{xyz_i}\right|$ and gyroscope $\left|G_{xyz_i}\right|$ signals are shown in Fig. 8. From $\left|A_{xyz_i}\right|$ and $\left|G_{xyz_i}\right|$, we found that data were normally distributed.

The A_{xyz} and G_{xyz} signals were then filtered by the *Savitzky-Golay (SG)* filter [38] to get A_{sg} and G_{sg}. This filter tends to filter out a significant portion of the original signal's high frequency content along with the noise and minimized the error by fitting a polynomial to frames of noisy data. A_{xyz}, G_{xyz}, A_{sg} and G_{sg} are then shifted to the center shown in Fig. 9.

B. Velocity and Distance Calculation

The accelerometer gives information about acceleration, velocity and position. There are some discrete integration methods available to perform numerical integration and a list of distance estimation approaches can be seen from Truong *et al.* [52]. During walking, horizontal distance can

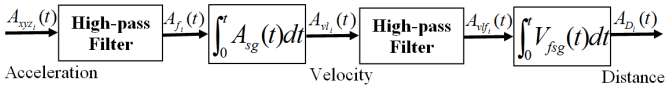

Fig. 10. Double integral process [60].

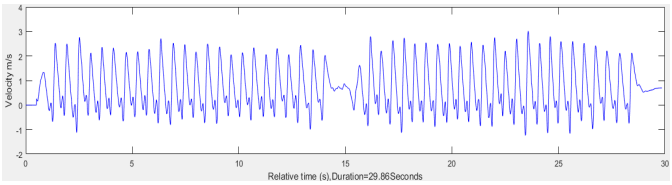

Fig. 11. Velocity A_{vl} after first integral.

be obtained by integrating the acceleration. In this analysis, the distance travelled by walking is obtained principally from the trapezoidal double integration method [60] of the user movement accelerometer signal A_{xyz} in the walking direction. There are two main problems for performing this, unknown initial condition and drift. Integration of the acceleration signal will generate a drift error. This can lead to large integration errors. The output can be unbound over time if the acceleration signal is integrated without filtering [60]. The integration works properly with known initial conditions. Thus, to calculate the actual displacement, integration errors must be minimized. As the displacement signal emphasizes the low frequency data more than the acceleration signal, the input A_{xyz} data were passed through a high-pass filter to remove the DC component of the acceleration signal. The double integral process is shown in Fig. 10 for calculating travelled distance.

In order to obtain the velocity and distance in time series, two stages of integration and two stages of high-pass filtering were applied. A second-order *od=2* Butterworth high-pass filter was designed with sampling frequency *fs=50 Hz*, cut off frequency *fc=1000 Hz*. The Butterworth filter was used with *fc* and *od* which have a magnitude response that is maximally flat in the bandpass and monotonic overall. This smoothness comes at the price of decreased roll off steepness. The output from Butterworth filter was then passed to *filtfilt* filter. The *filtfilt* corrected for phase distortion introduced by a one-pass filter, though it does square the magnitude response in the process [61]. The first integral operation *cumtrapz* in Matlab was applied on A_f data with respect to time t that gave the A_{vl} velocity (Fig. 11).

Linear trends were removed using *detrend* function by computing the least-squares fit of a straight line to the data and subtracted the resulting function from the data. A_{vl} was then passed through the high-pass filter for the second time and then the distance A_D was estimated after a second integral operation that is shown in Fig. 12.

The double integral process was then applied to estimate the walking distance. The result is presented in Table 1.

The highest accuracy 99.36% was found at location 5. The second best accuracy was found at location 1 (99.05%) followed by location 2, location 3 and location 4. The period of walking was using the android app. The estimated walking speed varied from 1.35 m/s to 2.29 m/s depending on

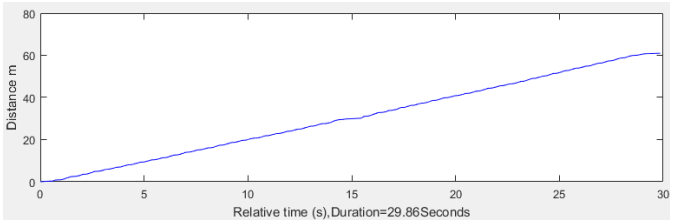

Fig. 12. Distance A_D after second integral.

TABLE I
DISTANCE AND SPEED CALCULATION

SL	RD (m)	ED (m)	Accuracy (%)	Period (s)	ES (m/s)
1	60.96	60.38	99.05	29.86	2.02
2	60.96	55.11	90.40	29.86	1.85
3	60.96	68.24	88.06	29.86	2.29
4	60.96	40.46	66.37	29.86	1.35
5	60.96	61.35	99.36	29.86	2.05

RD=Real Distance, ED=Estimated Distance, ES=Estimated Speed

the location. These results are consistent with human walking speed 1.5m/s to 2.5m/s previously documented in [62] and [63].

To validate our results, using 10 participants (age average 27.55 ± 3.54), we conducted trials using the Qualisys motion capture instrument (Qualisys Medical AB, Gothenburg, Sweden) [64] and from our IMU sensor concurrently. We applied our method to the collected data and the result is presented in Table 2. The average accuracy of our result is 97.77% with 95% confidence interval 0.767 for Est and 99.01% with 95% confidence interval 0.266 for Period.

C. Stride Event Detection

Human walking can be described and characterized in the context of a gait cycle. A stride is the equivalent of a gait cycle and is made-up of two steps. Each stride contains a stance and swing phases. Stance is comprised of five gait phases (initial contact, loading response, mid stance, terminal stance, pre-swing) and swing is comprised of three gait phases (initial swing, mid-swing and terminal swing). Stance and swing phases of a gait cycle consist of eight relevant phases shown in Fig. 13. During the stance phase, the foot initially contacts with ground. The loading response begins at the initial contact and ends when the opposite toe leaves the ground. The mid-stance begins at the end of the loading response and finishes when the center of gravity is over the reference foot. The terminal stance begins when the center of gravity is over the supporting foot and ends when the opposite contacts the ground. At the terminal stance, the heel rises from the ground. The pre-swing begins when the opposite is at the initial contact and ends at toe off. The period from the initial contact to pre-swing composes about 60% and initial swing and terminal swing composes about 40% of the gait cycle shown clearly in Fig. 13. As each stride consists of stance and swing events, thus the initial contact and the border between pre-swing and initial swing were detected to get stance and swing information.

TABLE II
VALIDATION OF OUR RESULTS WITH QUALISYS

Par	Leg	Qua	Est		Qua	Period	
		Distance(m)		Acry(%)	Time(s)		Acry(%)
1	Right	7.65	7.54	98.56	12.67	12.51	98.74
	Left	7.52	7.41	98.54	12.33	12.33	100.00
2	Right	7.4	7.01	94.73	12.67	12.83	98.74
	Left	7.46	7.24	97.05	12.33	12.28	99.59
3	Right	8.18	8.08	98.78	8.72	8.74	99.77
	Left	7.98	7.51	94.11	8.28	8.15	98.43
4	Right	7.98	7.68	96.24	8.72	8.88	98.17
	Left	8.12	7.97	98.15	8.28	8.18	98.79
5	Right	7.74	7.69	99.35	9.78	9.75	99.69
	Left	7.84	7.74	98.72	9.72	9.64	99.18
6	Right	7.56	7.45	98.54	9.78	9.71	99.28
	Left	7.48	7.56	98.93	9.72	9.83	98.87
7	Right	6.69	6.44	96.26	7.38	7.25	98.24
	Left	6.63	6.75	98.19	7.03	7.13	98.58
8	Right	6.42	6.71	95.48	7.38	7.31	99.05
	Left	6.14	6.22	98.70	7.03	7.14	98.44
9	Right	7.77	7.72	99.36	7.94	7.91	99.62
	Left	7.76	7.51	96.78	7.87	8.00	98.35
10	Right	7.51	7.46	99.33	7.94	7.96	99.75
	Left	7.62	7.59	99.61	7.87	7.80	99.11

Par= Participant No, Qua= Qualisys System, Est= Estimated distance using our method, Period=Total time of travelling the distance, Acry(%)=Accuracy in percentage

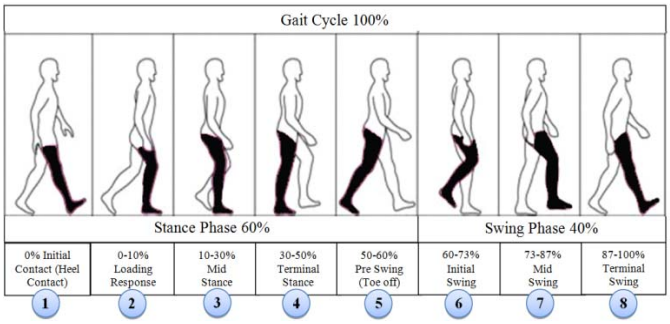

Fig. 13. Normal human gait phases [65].

These different phases of gait cycle were identifiable from IMU acceleration data (Fig. 13). The gait cycle signal patterns from literature accelerometer data [65], [66] and literature gyroscope data [67], [68] were compared to our gait cycle signal patterns ie the different phases labelled in Fig. 14 with the corresponding accelerometer data are shown in Fig. 13.

As we can see from Fig. 14 that the mid-swing phase in accelerometer and gyroscope data is a reliable indicator for the performance of the gait cycle, we chose this mark for counting the number of strides. The number of mid-swing phases in the accelerometer data was therefore equal to the number of strides.

Researchers used a variety of methods [37] for stride event detection from IMU sensors. During human walking, a consistent sequence of motions is performed at each stride that results in a maximum peak value in the mid-swing phase. This mid-swing phase appears when the person lifts up his/her

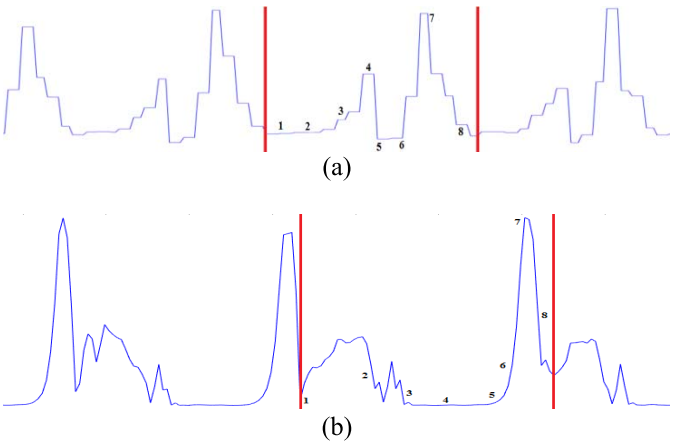

Fig. 14. Eight different phases of a gait cycle from (a) accelerometer data and (b) gyroscope data.

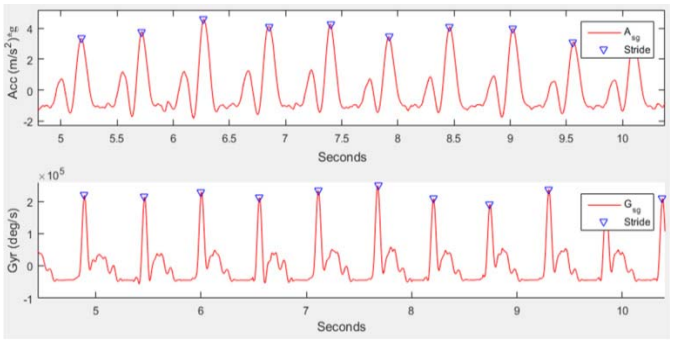

Fig. 15. Strides detection from accelerometer and gyroscope data.

foot, shortening the limb to clear the ground, releasing the foot until it is again in contact with the ground. A particular threshold value is set to detect these characteristics for [69]–[71]. A disadvantage of these methods is that any motion with a similar periodicity of walking will trigger off a false stride event. Difficulty arises to find the automatic selection of the threshold value which can vary between users, surfaces and shoes [72]. Most of these studies were carried under laboratory conditions [41] and tested on a relatively small number of subjects [37].

From Gyroscopic data the highest peak occurs at the mid-swing at the 7th phase (Fig. 13). Figure 8 shows that terminal stance and mid-swing events have very similar amplitudes. Applying a threshold based method to detect the stride number has a low accuracy as it detects two strides instead of single stride.

To perform the analysis, the characteristics of local maximal prominences of A_{sg} and G_{sg} were estimated through to a MATLAB built-in function (*findpeaks*) [73]. The *findpeaks* finds local peaks in the data vector and ignores small peaks that occur in the neighbourhood of a larger peak. It returned two vectors with the peaks (local maximal) and locations at which the peaks occur. A local peak was a data sample that was either larger than its two neighbouring samples or is equal to *Inf*. If a peak was flat, the function returns only the point with the lowest index. The outputs of these steps are shown in Fig. 15. The blue triangles show mid-swing phases for accelerometer (upper plot) and gyroscope (lower plot) in each stride.

TABLE III

STRIDE DETECTION ACCURACY FROM ACCELEROMETER AND GYROSCOPE DATA

Stride Number Estimation				
SL	SN_{Acc}	$Accuracy_{Acc}$	SN_{Gyr}	$Accuracy_{Gyr}$
1	48	96%	50	100%
2	43	86%	46	92%
3	48	96%	49	98%
4	48	96%	48	96%
5	50	100%	50	100%

SL=Sensor Location, SN=Stride Number

TABLE IV

STRIDE LENGTH AND PERIOD FOR SUBJECT 1

Stride Information				
	Length (m)		Period (s)	
SL	M	SD	M	SD
1	1.042	0.134	0.509	0.077
2	1.543	0.313	0.485	0.098
3	0.541	0.166	0.434	0.133
4	0.917	0.163	0.476	0.085
5	0.904	0.247	0.453	0.124

M=Mean, SD=Standard Deviation

These strides contain two arrays, one containing amplitude A_P, G_P in m/s^2 (peaks) and the time of those amplitudes A_L, G_L in *Time(t)* (locations) for corresponding accelerometer and gyroscope data. The number of A_P andG_P gave the number of strides.

The accuracy of the stride number estimated from five locations was computed using equation (7) and compared to the offline measured values shown in Table 3.

The accuracy for both accelerometer and gyroscope data is estimated using equation (7) where $ActualStride = 50$.

$$Accuracy = \begin{cases} \dfrac{StrideNumber_{Acc}}{ActualStride} \times 100\% \\ \quad if(ActualStride \geq StrideNumber_{Acc}) \\ \dfrac{100 - StrideNumber_{Acc}}{ActualStride} \times 100\% \\ \quad Otherwise \end{cases} \quad (7)$$

From Table 3, the highest detection is 100% from both acceleration and gyroscope data at location 5 which was over the insertion of the Achilles tendon into the calcaneum. The sensor orientation was also at a phase of 90 degree with the earth frame that gave significant information of each stride. The second best result was 96% from accelerometer and 100% from gyroscope data at location 1 (medial aspect of foot over the bony prominence of the first cuneiform). The sensor orientation and location of this place was the most stable as it was over a bone and relative movement is low. The third and fourth best locations were location 3 and 4 where the sensor orientation was tilted and the relative movement was high. The stride information of test subject 1 is presented in Table 4.

The standard deviations of the mean length and the mean period from location 1 were the lowest compared to location 2 to 5. Location 1 was therefore the more consistent and stable location. Location 2 had the highest standard deviation for mean length and location 3 for mean period indicating that these locations had more variation and poorer reliability.

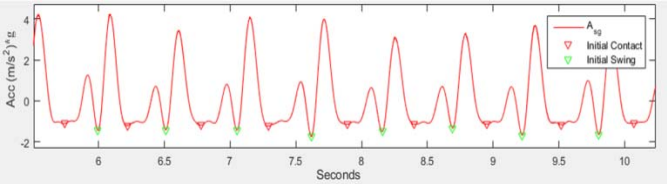

Fig. 16. Stance and swing phases.

TABLE V

STANCE LENGTH, PERIOD AND RATIO FOR SUBJECT 1

Stance Information					
	Length (m)		Period (s)		% of Stride
SL	M	SD	M	SD	
1	0.555	0.011	0.271	0.057	53.214
2	0.560	0.012	0.176	0.038	36.292
3	0.196	0.054	0.157	0.044	36.178
4	0.534	0.010	0.278	0.053	58.309
5	0.526	0.014	0.264	0.074	58.245

M=Mean, SD=Standard Deviation

TABLE VI

SWING LENGTH, PERIOD AND RATIO FOR SUBJECT 1

Swing Information					
	Length (m)		Period (s)		% of Stride
SL	M	SD	M	SD	
1	0.488	0.010	0.238	0.051	46.786
2	0.983	0.025	0.309	0.079	63.708
3	0.345	0.012	0.277	0.098	63.822
4	0.382	0.008	0.198	0.042	41.691
5	0.377	0.010	0.189	0.051	41.755

M=Mean, SD=Standard Deviation

D. Stance and Swing Events Detection

The stance and swing events were then detected by finding the local minima prominences before and after each mid-swing from A_P, and A_L using function *findpeaks*. A loop from 1 to total stride number was used to find each stance and swing events for each stride. The output to extract stance and swing phases is shown in Fig. 16.

In natural walking, the foot is on the ground for a little more than 60% of the total gait cycle referred as stance phase. A stance length is the distance between the heel contact and pre-swing phases and stance period is the interval of stance length. The stance information of test subject 1 is presented in Table 5. During the remainder of the gait cycle which is around 40%, the foot is off the ground as the limb is swung forward to begin the next stride referred as the swing phase. A swing length is the distance between the initial swing and terminal swing phases and the swing period is the interval of swing length. The swing information of test subject 1 is presented in Table 6.

Using the stride and distance data, our method is used to estimate stance and swing phase movement information shown in Tables 5-6.

Stance is the first part of a stride. The standard deviations of length and period for stance and swing are low (Table 5).

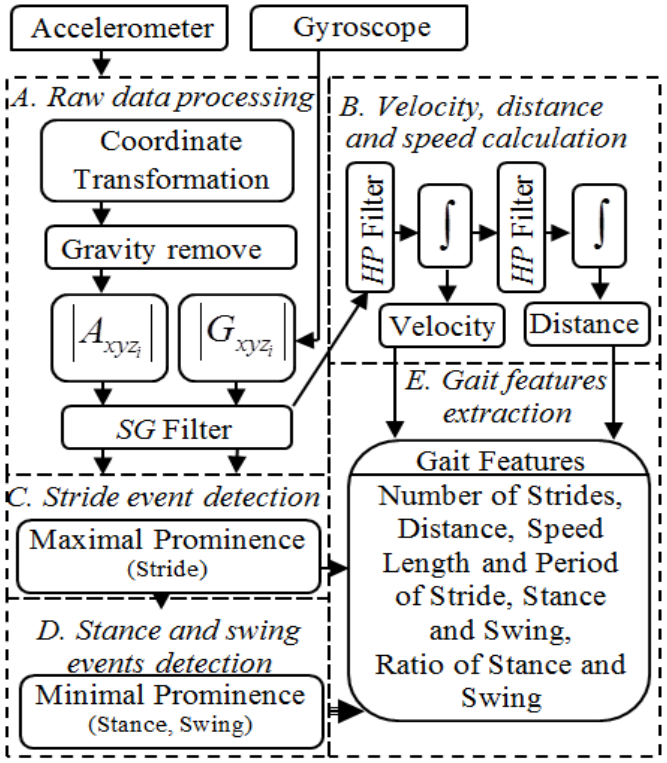

Fig. 17. The process diagram of the automatic features extraction from accelerometer and gyroscope.

The highest % of stride is found at location 5 and location 4. According to the literature the stance and swing ratio is 60:40% of the stride location 5 and 4 are close to 60:40 % split of the stride for this subject. Although location 5 shows close to 60% of the stride for this subject, statistical information for this will be conducted in section IV experiment and discussion.

E. Gait Features Extraction

Number of stride, travelled distance, speed, stride length, stride period, stance length, stance period, swing length and swing period and the ratio of stance and swing were estimated from the method described above. To summarize the above discussion, our proposed gait features extraction method is shown in Fig. 17.

IV. Experiments and Discussion

In this section, we applied the method developed in section III from one participant to 15 participants. We present the results to demonstrate our proposed method statistically and the discussion.

A. Experiments

The procedure for gait features extraction was conducted for a total of 10 male and 5 female participants (mean age: 25.3 years (19 to 35), weight: 60.7 kg and height: 1.658 meter) were recruited for this investigation.

Table 7 shows the average stride number detected for 15 participants. The highest accuracy for the detection of stride count from accelerometer and gyroscopic data is in location 1

TABLE VII
AVERAGE STRIDE DETECTION ACCURACY FOR 15 SUBJECTS

Average Stride Number Estimation				
SL	SN_{Acc}	$Accuracy_{Acc}$	SN_{Gyr}	$Accuracy_{Gyr}$
1	47.73	95.47%	46.80	93.60%
2	45.07	90.13%	46.33	92.66%
3	44.93	89.87%	46.40	92.80%
4	47.00	94.00%	46.53	93.06%
5	47.40	94.80%	46.60	93.20%

SL=Sensor Location, SN=Stride Number

closely followed by locations 5 and 4. Although, location 5 gave the highest accuracy during the method development in section III, with more participants location 1 shows the best result in being the closest to correlate estimated distance travelled to measured (actual) distance travelled (Table 8) and is also closest to the 60:40% split for average stride, stance and swing information (Table 9).

We checked the data for statistical errors and assessed whether the estimated values were reasonable. A boxplot of stride number estimation and accuracy of detection from accelerometer and gyroscope data for location 1 to location 5 bfrom 15 participants is presented in Fig. 18. It is to be noted that the observations identified by the boxplots are not especially extreme. Our method to detect the stride number from location 1 to location 5 shows about 45±5 strides with accuracy of about 90±5% for accelerometer and accuracy of about 90±10% for gyroscope data. The highest value of the average stride number estimation from the gyroscope is in location 1 but the data distribution is wider than other locations. The overall mean values of stride detection show that the IMU data collected from five different foot locations do not have a high variation from accelerometer data. However, the accelerometer data distribution of location 1 is more stable compared to the gyroscope data distribution showing it to be more reliable for gait analysis. Location 5 of gyroscope data shows a good data capture. Based on these observations, location 1 appeared to be the most stable to collect reliable and quality data from an accelerometer for lower limb gait analysis.

The average real and estimated distance travelled by 15 participants, their accuracy, period of walking and estimated speed information with confidence intervals from location 1 to location 5 are presented in Table 8. The average estimated walking speed from young participants varies from 1.35m/s to 1.46m/s. The highest accuracy of distance estimation is found from location 1 with an accuracy of 95.24% followed by location 5, location 2, location 3 and location 4.

The total real and estimated distances for performing 25 strides of normal walking, a turn-around and another 25 strides, traveling period and speed summary are presented in Fig. 19.

Due to different age groups, height and walking style, participants walked from 45m to 70m to complete a total of 50 strides. The real distance and the estimated distance are very close in the dataset with average accuracy is more than 90%. The average stride, stance and swing phase information for 15 participants are presented in Table 9.

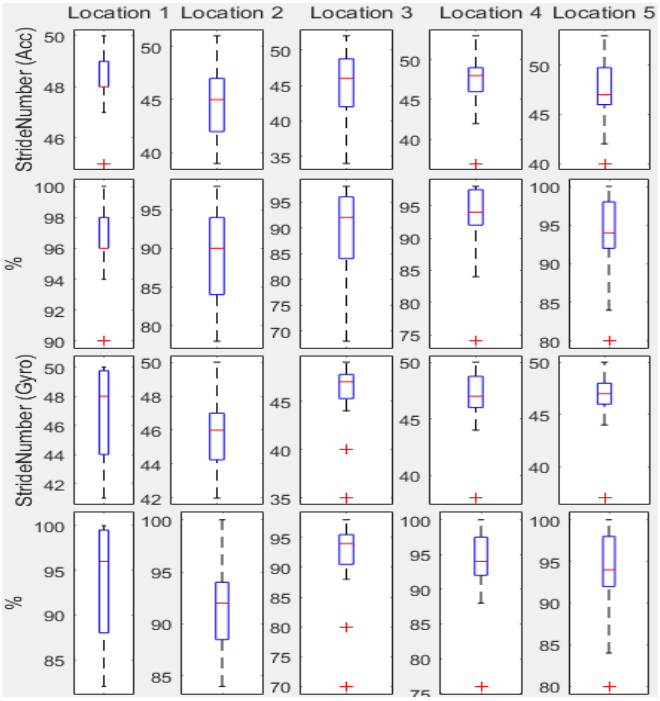

Fig. 18. Boxplot of Stride number estimation and accuracy of detection from Accelerometer and Gyroscope data for location 1 to location 5 from 15 participants.

TABLE VIII

ACCURACY AND CONFIDENCE INTERVAL OF DISTANCE AND SPEED FOR 15 SUBJECTS

Average Distance and Speed calculation									
SL	RD (m)	ED (m)	(%)	95% CI		P(s)	ES (m/s)	95% CI	
1	59.21	58.45	95.24	56.05	60.84	41.22	1.40	1.24	1.56
2	59.21	60.10	85.95	58.12	62.09	41.22	1.46	1.27	1.65
3	59.21	56.46	85.87	52.95	59.98	41.22	1.37	1.17	1.58
4	59.21	56.68	85.06	53.68	59.67	41.22	1.38	1.20	1.56
5	59.21	56.01	90.85	53.65	58.37	41.22	1.35	1.18	1.52

RD=Real Distance, ED=Estimated Distance, (%) =Accuracy, P=Period, ES=Estimated Speed, CI=Confidence Intervals

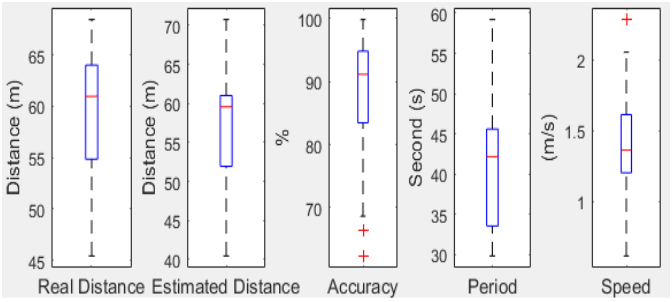

Fig. 19. Boxplot of real and estimation distance, their accuracy, period and speed from accelerometer data for location 1 to location 5.

The calculated average stride was based on heel to heel contact. The length and period from location 1 to 5 varies low and for normal walking, the stride length varies from person to person. Location 1 was closest to the 60:40% split for stance : swing that agrees with the literature [65], [74].

The individual participant information including anthropometric characteristics is provided with the supporting document.

TABLE IX

STRIDE, STANCE AND SWING INFORMATION FOR 15 SUBJECTS

SL	Average Stride		Average Stance			Average Swing		
	L (m)	P (s)	L (m)	P (s)	% S	L (m)	P (s)	% S
1	1.104	0.503	0.649	0.259	59.501	0.455	0.244	40.499
2	1.304	0.460	0.659	0.229	63.705	0.413	0.228	48.169
3	1.251	0.468	0.614	0.228	56.438	0.465	0.238	51.013
4	0.971	0.512	0.499	0.261	82.399	0.372	0.247	47.225
5	1.223	0.503	0.621	0.255	49.907	0.590	0.244	48.782

L=Length, P=Period, % S=% of Stride

B. Discussion

From the above results, this study has shown that placing an IMU sensor at location 1 located on the medial aspect of foot over the bony prominence of the first cuneiform maximizes the accuracy of the collected accelerometer and gyroscope data. In this location the sensor offers the best performance to identify the stride count, calculated distance and average stride, stance and swing information. Location 1 is closely followed by locations 5 and 4. This may well be because it is easier to secure the sensor at these locations. Sensor locations 1 and 5 have less relative movement; locations 4 and 3 have slight movement during walking time while location 2 has movement due to expansion and squeezing of the foot during step movement. Location 3 also has an angular orientation when the sensor is placed that cancels the prominent data.

We have identified that placing the sensor on different locations of the foot parts affects sensor output. It is also noted that the orientation of the sensor has a significant effect on output data and placing the sensor in different locations gives a different pattern to the data. If data are to be collected regularly, the position and orientation of the sensor are crucial as changes in position through human error may give different data patterns which might be difficult to interpret. This highlights the importance of properly fixing the sensor to the optimal location to avoid inaccuracies.

Other possible areas of error may arise from frictional noise and the relative movement of clothing and shoes to the sensor. The placing of sensors on foot locations requires other generic considerations such as battery life and android device that is BLE enable to pick up sensor data.

In order to track the position in a virtual environment, several navigation methods [75] are available to derive pose estimates from electrical measurements of mechanical, inertial, acoustic, magnetic, optical, and radio frequency sensors. Each approach has advantages and limitations including modality-specific limitations related to the physical medium, measurement-specific limitations imposed by the devices, associated signal-processing electronics, and circumstantial limitations that arise in a specific application [76].

Our distance estimation method is based on results of a double integral of acceleration data and removes linear trend from the signal to estimate distance. We used the simplest technique of trapezoidal rule for estimating distance for our collected data and our estimated distance results are close to the actual distance. There are many other types of numerical integration schemes available which are much more involved

and with the potential for more accuracy. However, the trapezoidal rule is the simplest technique of an entire class of numerical integration schemes which is known as the *Newton-Cotes Formulas* [77] and which we have adopted. Our future plan is to investigate other methods with our collected data.

Our proposed method for detecting stride information is based on local maxima, stance and swing event information is based on local minima prominence characteristics instead of conventional threshold based detections mentioned in section III.*B*. We found that that when turning or when stopping there is a poor acceleration signal. For this reason, we used local maxima or minima prominence characteristics to detect different events to avoid these crucial phases. We have shown that it is possible to detect, stride, stance and swing event but further analysis of the eight events in a gait cycle is necessary to provide more accurate information of gait pattern. Automatic gait features (stride number, distance, speed, length and period of stride, stance and swing) extracted from accelerometer and gyroscope data can be used to identify and monitor abnormal gait patterns changes over time. They can provide real time monitoring of patients. This has considerable potential for future developments to identify long time gait pattern changes and explore ways how these features can be useful for fall risk assessment in an elderly population. This study has shown that this is possible.

There are however a number of limitations. The number of subjects is small (10 male and 5 female). There is the potential of a Type 1 error in detecting an effect that is not there. In addition our subjects were walking barefoot and it was not possible to wear a shoe over the sensor as this would have caused discomfort. However our work can be considered a proof of concept study that has established our method for extracting automatic gait features.

We have shown that our method is capable of extracting these automatic features and has the potential to be used in assessment of gait, gait change monitoring, gait asymmetry and clinical use associated with gait pattern. Gait with slow velocity is common in elderly people [78] and gait analysis where the gait cycle is relatively slower compared to young adult. Our low cost portable personalized proposed solution could bring out automatic gait features for monitoring longitudinal gait changes or abnormalities. In future works, we plan to use our automatic extracted gait features information to classify gait changes over time to identify abnormal gait patterns for the assessment of elderly fall risk, rehabitation and sports applications.

V. Conclusion

In our study we have found the optimal location on the foot for placing an IMU sensor. We have developed a mobile phone app for synchronised data collection from a low cost MetaWear CPro sensor. We also proposed a method for automatic gait features and present our own real time physical data.

The influence of IMU sensor orientation and sensor placement on different foot locations had been investigated to improve the accuracy for gait analysis. The IMU accelerometer and gyroscope data had been analysed using our method to extract ten automatic features: Number of Strides, Distance, Speed, Stride Length, Stride Period, Stance Length, Stance Period, Swing Length, Swing Period and ratio of stance and swing. The trapezoidal rule based double integrating technique was applied on acceleration data to estimate the horizontal displacement of the foot and compared the result with actual distance in the real world. Our study shows that the sensor orientation and small changes of sensor location influence the sensor output. The results show that location 1 over the bony prominence of the first cuboid bone is the best place for placing a sensor as it delivers the most accurate data. This location is also the centre point of foot length. The sensor is attached with a Velcro elastic belt and buckles to adjust the fitting. As the sensor is attached on bone the relative movement between the sensor frame and foot frame is assumed to be zero. Currently, the proposed method is only applied on estimating distance of normal walking on ground level and this method will be extended to assessment of gait, gait change monitoring, gait asymmetry and clinical use associated with gait pattern. The comparison between the real and estimated distance and speed shows a good agreement with low errors which shows that these features could be used for gait analysis in a normal daily living environment. Our future work will aim to use our automatic extracted gait features information to classify long term gait pattern changes for identifying abnormal gait patterns for the assessment of elderly fall risk, rehabilitation and sports applications.

Ethical Approval

Ethical approval for this research was granted by the Bournemouth University ethical review committee and each subject was given a Participant Information Sheet and signed an informed Participant Agreement Form.

Acknowledgement

The authors would like to thank Dr Andrew Callaway for his help to collect data from Qualisys and all participants that participated in the study.

References

[1] A. Muro-De-La-Herran, B. Garcia-Zapirain, and A. Mendez-Zorrilla, "Gait analysis methods: An overview of wearable and non-wearable systems, highlighting clinical applications," *Sensors*, vol. 14, no. 2, pp. 3362–3394, 2014.

[2] Y. Wahab and N. A. Bakar, "Gait analysis measurement for sport application based on ultrasonic system," in *Proc. IEEE 15th Int. Symp. Consum. Electron. (ISCE)*, Jun. 2013, pp. 20–24.

[3] M. P. M. Steultjens, J. Dekker, M. E. van Baar, R. A. B. Oostendorp, and J. W. J. Bijlsma, "Range of joint motion and disability in patients with osteoarthritis of the knee or hip," *Rheumatology*, vol. 39, no. 9, pp. 955–961, 2000.

[4] N. M. Bora, G. V. Molke, and H. R. Munot, "Understanding human gait: A survey of traits for biometrics and biomedical applications," in *Proc. Int. Conf. Energy Syst. Appl.*, 2015, pp. 723–728.

[5] J. M. Hausdorff, D. A. Rios, and H. K. Edelberg, "Gait variability and fall risk in community-living older adults: A 1-year prospective study," *Arch. Phys. Med. Rehabil.*, vol. 82, no. 8, pp. 1050–1056, Aug. 2001.

[6] B. E. Maki, "Gait changes in older adults: Predictors of falls or indicators of fear?" *J. Amer. Geriatrics Soc.*, vol. 45, no. 3, pp. 313–320, 1997.

[7] V. Bianchi, "Fall detection and gait analysis in a smart home environment," *Gerontechnology*, vol. 7, no. 2, p. 73, 2008.

[8] S. A. Bridenbaugh and R. W. Kressig, "Laboratory review: The role of gait analysis in seniors mobility fall prevention," *Gerontology*, vol. 57, no. 3, pp. 256–264, 2011.

[9] J. Verghese, C. Wang, R. B. Lipton, R. Holtzer, and X. Xue, "Quantitative gait dysfunction and risk of cognitive decline and dementia," *J. Neurol. Neurosurg. Psychiatry*, vol. 78, no. 9, pp. 929–935, Sep. 2007.

[10] S. Marquis *et al.*, "Independent predictors of cognitive decline in healthy elderly persons," *Arch. Neurol.*, vol. 59, no. 4, pp. 601–606, 2002.

[11] A. M. Shelat, *Evidence-Based Physical Diagnosis*, 3rd ed. U.S. National Library of Medicine, Bethesda, MD, USA, Jun. 2016. [Online]. Available: https://www.nlm.nih.gov/medlineplus/ency/article/003199.htm

[12] B. F. L. van Nuenen *et al.*, "Postoperative gait deterioration after bilateral subthalamic nucleus stimulation in Parkinson's disease," *Movement Disorders*, vol. 23, no. 16, pp. 2404–2406, 2008.

[13] B. R. Bloem, J. Gussekloo, A. M. Lagaay, E. J. Remarque, J. Haan, and R. G. J. Westendorp, "Idiopathic senile gait disorders are signs of subclinical disease," *J. Amer. Geriatrics Soc.*, vol. 48, no. 9, pp. 1098–1101, Sep. 2000.

[14] R. G. T. Khan. (Jul. 2016). *Gait Alterations Associated With Diabetic Neuropathy|Lower Extremity Review Magazine*. [Online]. Available: http://lermagazine.com/article/gait-alterations-associated-with-diabetic-neuropathy

[15] A. H. Snijders, B. P. van de Warrenburg, N. Giladi, and B. R. Bloem, "Neurological gait disorders in elderly people: Clinical approach and classification," *Lancet Neurol.*, vol. 6, no. 1, pp. 63–74, 2007.

[16] J. S. Brach and J. M. VanSwearingen, "Physical impairment and disability: Relationship to performance of activities of daily living in community-dwelling older men," *Phys. Therapy*, vol. 82, no. 8, pp. 752–761, 2002.

[17] R. J. Hess, J. S. Brach, S. R. Piva, and J. M. VanSwearingen, "Walking skill can be assessed in older adults: Validity of the figure-of-8 walk test," *Phys. Therapy*, vol. 90, no. 1, pp. 89–99, 2010.

[18] R. P. Duncan and G. M. Earhart, "Four square step test performance in people with Parkinson disease," *J. Neurol. Phys. Therapy*, vol. 37, no. 1, pp. 2–8, Mar. 2013.

[19] D. M. Wrisley and N. A. Kumar, "Functional gait assessment: Concurrent, discriminative, and predictive validity in community-dwelling older adults," *Phys. Therapy*, vol. 90, no. 5, pp. 761–773, 2010.

[20] W. J. R. Bossers, L. H. V. van der Woude, F. Boersma, E. J. A. Scherder, and M. J. G. van Heuvelen, "The Groningen meander walking test: A dynamic walking test for older adults with dementia," *Phys. Therapy*, vol. 94, no. 2, pp. 262–272, 2014.

[21] K. O. Berg, S. L. Wood-Dauphinee, J. I. Williams, and B. Maki, "Measuring balance in the elderly: Validation of an instrument," *Can. J. Public Health*, vol. 83, no. 2, pp. 7–11, 1992.

[22] V. Agostini, M. Knaflitz, L. Antenucci, G. Lisco, L. Gastaldi, and S. Tadano, "Wearable sensors for gait analysis," in *Proc. IEEE Int. Symp. Med. Meas. Appl. (MeMeA)*, May 2015, pp. 146–150.

[23] R. Hanly, F. Doyle, S. Whitehouse, and A. J. Timperley, "Outpatient 3-D gait analysis one year after THA using a portable IMU system," *Orthopaedic Proc.*, vol. 98-B, no. 11, p. 1, 2016.

[24] N. Shibuya *et al.*, "A real-time fall detection system using a wearable gait analysis sensor and a support vector machine (SVM) classifier," in *Proc. ICMU*, Jan. 2015, pp. 66–67.

[25] S. M. Rispens *et al.*, "Fall-related gait characteristics on the treadmill and in daily life," *J. Neuroeng. Rehabil.*, vol. 13, no. 1, pp. 1–9, 2016.

[26] S. Okuda *et al.*, "Gait analysis of patients with Parkinson's disease using a portable triaxial accelerometer," *Neurol. Clin. Neurosci.*, vol. 4, no. 3, pp. 93–97, 2016.

[27] S. A. Fouaz, H. P. Nguyen, C. Lavigne-Pelletier, E. Goubault, P. Boissy, and C. Duva, "Wavelet-based algorithm for auto-detection of daily living activities of older adults captured by multiple inertial measurement units (IMUs)," *Physiol. Meas.*, vol. 37, no. 3, p. 442, 2016.

[28] N. Kitagawa and N. Ogihara, "Estimation of foot trajectory during human walking by a wearable inertial measurement unit mounted to the foot," *Gait Posture*, vol. 45, pp. 110–114, Mar. 2016.

[29] C. E. Matthews, M. Hagströmer, D. M. Pober, and H. R. Bowles, "Best practices for using physical activity monitors in population-based research," *Med. Sci. Sports Exerc.*, vol. 44, no. 1, pp. S68–S76, 2012.

[30] C. V. Bouten, A. A. H. J. Sauren, M. Verduin, and J. D. Janssen, "Effects of placement and orientation of body-fixed accelerometers on the assessment of energy expenditure during walking," *Med. Biol. Eng. Comput.*, vol. 35, no. 1, pp. 50–60, Jan. 1997.

[31] G. Plasqui and K. R. Westerterp, "Physical activity assessment with accelerometers: An evaluation against doubly labeled water," *Med. Obesity*, vol. 15, no. 10, pp. 2371–2379, Oct. 2007.

[32] S. S. Intille, J. Lester, J. F. Sallis, and G. Duncan, "New horizons in sensor development," *Med. Sci. Sports Exerc.*, vol. 44, no. 1, pp. S24–S31, Jan. 2012.

[33] J. A. Lee, S.-H. Cho, J.-W. Lee, K.-H. Lee, and H.-K. Yang, "Wearable accelerometer system for measuring the temporal parameters of gait," in *Proc. EMBS*, 2007, pp. 483–486.

[34] P. C. Chung, Y.-L. Hsu, C.-Y. Wang, C.-W. Lin, J.-S. Wang, and M.-C. Pai, "Gait analysis for patients with Alzheimer'S disease using a triaxial accelerometer," in *Proc. ISCAS*, 2012, pp. 1323–1326.

[35] J. J. Kavanagh, "Lower trunk motion and speed-dependence during walking," *J. Neuroeng. Rehabil.*, vol. 6, no. 1, p. 9, 2009.

[36] Y. Song, S. Shin, S. Kim, D. Lee, and K. H. Lee, "Speed estimation from a tri-axial accelerometer using neural networks," in *Proc. EMBS*, 2007, pp. 3224–3227.

[37] A. Brajdic and R. Harle, "Walk detection and step counting on unconstrained smartphones," in *Proc. ACM Int. Joint Conf. Pervasive Ubiquitous Comput.*, Zürich, Switzerland, 2013, pp. 225–234.

[38] M. Mladenov and M. Mock, "A step counter service for Java-enabled devices using a built-in accelerometer," in *Proc. 1st Int. Workshop Context-Aware Middlew. Services, Affiliated 4th Int. Conf. Commun. Syst. Softw. Middlew. (COMSWARE)*, Dublin, Ireland, 2009, pp. 1–5.

[39] R. C. Foster *et al.*, "Precision and accuracy of an ankle-worn accelerometer-based pedometer in step counting and energy expenditure," *Preventive Med.*, vol. 41, nos. 3–4, pp. 778–783, 2005.

[40] M. Boutaayamou *et al.*, "Development and validation of an accelerometer-based method for quantifying gait events," *Med. Eng. Phys.*, vol. 37, no. 2, pp. 226–232, 2015.

[41] J. R. Rebula, L. V. Ojeda, P. G. Adamczyk, and A. D. Kuo, "Measurement of foot placement and its variability with inertial sensors," *Gait Posture*, vol. 38, no. 4, pp. 974–980, 2013.

[42] M. Brandes, W. Zijlstra, S. Heikens, R. van Lummel, and D. Rosenbaum, "Accelerometry based assessment of gait parameters in children," *Gait Posture*, vol. 24, no. 4, pp. 482–486, 2006.

[43] J. M. Merryn, A. C. F. Coster, N. H. Lovell, and B. G. Celler, "Accelerometry: Providing an integrated, practical method for long-term, ambulatory monitoring of human movement," *Physiol. Meas.*, vol. 25, no. 2, p. R1, 2004.

[44] J. Markowitz and H. Herr, "Human leg model predicts muscle forces, states, and energetics during walking," *PLoS Comput. Biol.*, vol. 12, no. 5, p. e1004912, 2016.

[45] S. C. Mukhopadhyay, "Wearable sensors for human activity monitoring: A review," *IEEE Sensors J.*, vol. 15, no. 3, pp. 1321–1330, Mar. 2015.

[46] M. Cornacchia, K. Ozcan, Y. Zheng, and S. Velipasalar, "A survey on activity detection and classification using wearable sensors," *IEEE Sensors J.*, vol. 17, no. 2, pp. 386–403, Jan. 2017.

[47] D. Rodríguez-Martín, C. Pérez-López, A. Samà, J. Cabestany, and A. Català, "A wearable inertial measurement unit for long-term monitoring in the dependency care area," *Sensors*, vol. 13, no. 10, p. 14079, 2013.

[48] N. Hegde, M. Bries, and E. Sazonov, "A comparative review of footwear-based wearable systems," *Electron.*, vol. 5, no. 3, p. 48, 2016.

[49] E. S. Sazonov, G. Fulk, J. Hill, Y. Schutz, and R. Browning, "Monitoring of posture allocations and activities by a shoe-based wearable sensor," *IEEE Trans. Biomed. Eng.*, vol. 58, no. 4, pp. 983–990, Apr. 2011.

[50] K. Aminian *et al.*, "Estimation of speed and incline of walking using neural network," in *Proc. IEEE 10th Anniversary. Adv. Technol. I&Amp, M*, vol. 1. May 1994, pp. 160–162.

[51] Y. Hikihara, P. Robert, E. Jequier, and Y. Schutz, "Prediction models discriminating between nonlocomotive and locomotive activities in children using a triaxial accelerometer with a gravity-removal physical activity classification algorithm," *PLoS ONE*, vol. 9, no. 4, p. e94940, 2014.

[52] P. Truong, J. Lee, A.-R. Kwon, and G.-M. Jeong, "Stride counting in human walking and walking distance estimation using insole sensors," *Sensors*, vol. 16, no. 6, p. 823, 2016.

[53] *I. SolidWorks*, Solidworks Corp., Concord, MA, USA, 2002.

[54] J. Loudon, M. Swift, and S. Bell, *The Clinical Orthopedic Assessment Guide*, 2nd ed. Champaign, IL, USA: Human Kinetics, 2008, pp. 395–408.

[55] (Aug. 3, 2016). *MbientLab*. [Online]. Available: https://mbientlab.com/docs/MetaWearCPSv0.5.pdf

[56] S. O. H. Madgwick, "An efficient orientation filter for inertial and inertial/magnetic sensor arrays," *Citado*, vol. 5, pp. 9–19, Apr. 2010.

[57] R. Mahony, T. Hamel, and J.-M. Pflimlin, "Nonlinear complementary filters on the special orthogonal group," *IEEE Trans. Autom. Control*, vol. 53, no. 5, pp. 1203–1218, Jun. 2008.

[58] D. Mizell, "Using gravity to estimate accelerometer orientation," in *Proc. 7th IEEE Int. Symp. Wearable Comput.*, Oct. 2013, pp. 252–253.
[59] Starlino. (Apr. 2016). *A Guide to using IMU (Accelerometer and Gyroscope Devices) in Embedded Applications*. [Online]. Available: http://www.starlino.com/imu_guide.html
[60] Y. K. Thong, M. S. Woolfson, J. A. Crowe, B. R. Hayes-Gill, and D. A. Jones, "Numerical double integration of acceleration measurements in noise," *Measurement*, vol. 36, no. 1, pp. 73–92, 2004.
[61] A. V. Oppenheim and R. W. Schafer, *Discrete-Time Signal Processing*. Englewood Cliffs, NJ, USA: Prentice-Hall, 1989, pp. 311–312.
[62] B. J. Mohler, W. B. Thompson, S. H. Creem-Regehr, H. L. Pick, and W. H. Warren, "Visual flow influences gait transition speed and preferred walking speed," *Experim. Brain Res.*, vol. 181, no. 2, pp. 221–228, 2007.
[63] A. E. Minetti, *The Three Modes of Terrestrial Locomotion*. Champaign, IL, USA: Human Kinetics, 2000.
[64] (Aug. 4, 2017). *Qualisys Motion Capture*. [Online]. Available: https://www.qualisys.com/start/
[65] D.-X. Liu, X. Wu, W. Du, C. Wang, and T. Xu, "Gait phase recognition for lower-limb exoskeleton with only joint angular sensors," *Sensors*, vol. 16, no. 10, p. 1579, 2016.
[66] M. Patterson, E. Delahunt, K. T. Sweeney, and B. Caulfield, "An ambulatory method of identifying anterior cruciate ligament reconstructed gait patterns," *Sensors*, vol. 14, no. 1, p. 887, 2014.
[67] B. R. Greene, A. O. Donovan, R. Romero-Ortuno, L. Cogan, C. N. Scanaill, and R. A. Kenny, "Quantitative falls risk assessment using the timed up and go test," *IEEE Trans. Biomed. Eng.*, vol. 57, no. 12, pp. 2918–2926, Dec. 2010.
[68] F. Casamassima, A. Ferrari, B. Milosevic, P. Ginis, E. Farella, and L. Rocchi, "A wearable system for gait training in subjects with Parkinson's disease," *Sensors*, vol. 14, no. 4, p. 6229, 2014.
[69] P. Goyal, V. J. Ribeiro, H. Saran, and A. Kumar, "Strap-down pedestrian dead-reckoning system," in *Proc. IPIN*, 2011, pp. 1–7.
[70] J. W. Kim, H. J. Jang, D.-H. Hwang, and C. Park, "A step, stride and heading determination for the pedestrian navigation system," *Positioning*, vol. 3, nos. 1–2, pp. 273–279, 2004.
[71] C. Randell, C. Djiallis, and H. Muller, "Personal position measurement using dead reckoning," in *Proc. ISWC*, 2003, p. 17.
[72] D. Gafurov and E. Snekkenes, "Towards understanding the uniqueness of gait biometric," in *Proc. 8th IEEE Int. Conf. Autom. Face Gesture Recognit. (FG)*, Sep. 20098, pp. 1–8.
[73] (Dec. 14, 2016). *Find Local Maxima-MATLAB Findpeaks*. The MathWorks Inc. MathWorks United Kingdom. [Online]. Available: https://uk.mathworks.com/help/sisgnal/ref/findpeaks.html
[74] M. Iosa *et al.*, "The golden ratio of gait harmony: Repetitive proportions of repetitive gait phases," *BioMed Res. Int.*, vol. 2013, May 2013, Art. no. 918642.
[75] A. M. Hasan, K. Samsudin, A. R. Ramli, R. S. Azmir, and S. A. Ismaeel, "A review of navigation systems (integration and algorithms)," *Austral. J. Basic Appl. Sci.*, vol. 3, no. 2, pp. 943–959, 2009.
[76] G. Welch and E. Foxlin, "Motion tracking: No silver bullet, but a respectable arsenal," *IEEE Comput. Graph. Appl.*, vol. 22, no. 6, pp. 24–38, Nov. 2002.
[77] E. W. Weisstein. Newton-Cotes formulas. MathWorld—A Wolfram Web Resource. [Online]. Available: http://mathworld.wolfram.com/Newton-CotesFormulas.html
[78] J. S. Brach and J. M. VanSwearingen, "Interventions to Improve Walking in Older Adults," *Current Transl. Geriatrics Experim. Gerontol. Rep.*, vol. 2, no. 4, pp. 230–238, 2013.

Arif Reza Anwary received the B.Sc. degree in computer science and engineering from the University of Asia Pacific, Bangladesh, the M.Sc. degree in computer science from Gyeongsang National University, South Korea, and the M.Phil. degree in statistical shape analysis for the human back from the University of Wolverhampton, U.K. He is currently pursuing the Ph.D. degree with Bournemouth University. He was an Assistant Professor with the Department of Computer Science and Engineering, United International University, Bangladesh. His current research interest includes gait analysis, machine learning, and cognition for intelligent agents.

Hongnian Yu (SM'17) is currently a Professor of Computing with Bournemouth University and has extensive research experience in robotics, digital healthcare, mobile computing, modeling, scheduling, planning, and simulations, manufacturing systems, supply chains, computer networks and RFID applications, modeling and control of robots and mechatronics, and neural networks. He has successfully supervised 20 Ph.D. theses and 16 master's theses, and has trained 11 post-doctoral research fellows. He has published over 200 journals and conference research papers. He has held several research grants worth over eight million pounds from the U.K. EPSRC, the Royal Society, and the European AWM, as well as from industry. He is a member of the EPSRC Peer Review College and a Fellow of IET. He was a recipient of the F.C. William Premium for his paper on adaptive and robust control of robot manipulators by the IEEE Council, and has received one Best Conference Paper Award and five Best (Student) Conference Paper Awards with his research students. He has strong research collaboration with partners from many countries, such as China, France, Germany, Hungary, India, Italy, Japan, Romania, Thailand, and USA.

Michael Vassallo is currently a Consultant Geriatrician with the Royal Bournemouth Hospital, U.K. He has a research interest in falls and rehabilitation and has published widely in the area.